Available online at www.sciencedirect.com
ScienceDirect
Thermochimica Acta 470 (2008) 60–66
thermochimica acta
www.elsevier.com/locate/tca

Effect of TiO_2 addition on the crystallization and tribological properties of MgO–CaO–SiO_2–P_2O_5–F glasses

Jongee Park *, Abdullah Ozturk

Middle East Technical University, Metallurgical and Materials Engineering Department, Ankara 06531, Turkey

Received 9 July 2007; received in revised form 12 November 2007; accepted 26 January 2008
Available online 6 February 2008

Abstract

The kinetic parameters including the activation energy for crystallization (E), the Avrami parameter (n) and frequency factor (υ) of a glass in the MgO–CaO–SiO_2–P_2O_5–F system were studied using non-isothermal differential thermal analysis (DTA) with regard to small amount of TiO_2 additions. It has been shown that the role of TiO_2 changes from a glass network former to a glass network modifier with increasing TiO_2 content in this system. The kinetic parameters of the crystallizing phases, apatite and wollastonite, indicated changes accompanied with TiO_2 additions, implying that the TiO_2 is an effective nucleating agent for promoting the crystallization of apatite and wollastonite. The most effective addition is of about 4 wt% TiO_2 in this system. The wear rate and friction coefficient decreased from 1.8 ± 0.1 to 0.9 ± 0.2 and 0.87 to 0.77, respectively, when 4 wt% TiO_2 was incorporated to the base glass.

Keywords: Glass ceramics; TiO_2; Crystallization; Kinetics; Wear

1. Introduction

The discovery of the glass ceramics containing apatite [$Ca_{10}(PO_4)_6(O,F_2)$] and wollastonite [$CaO{\cdot}SiO_2$] crystals as the predominant crystalline phases in the MgO–CaO–SiO_2 glass matrix by Kokubo et al. [1] in 1982 has drawn attention principally due to their biological ability to bond spontaneously to living bone and their enhanced mechanical properties such as toughness and strength. Since then, apatite–wollastonite (A–W) glass ceramics have received great importance as a biomaterial in biomedical applications especially in the repair and replacement of natural bone [1–4].

The properties of A–W glass ceramics are related to the microstructure developed during heat treatment. This may have an influence on the wear properties of A–W glass ceramics. Wear of dental materials is a serious concern in clinical applications, especially when tooth enamel is in occlusal contact with a harder ceramic restoration material [5]. Jahanmir and Dong [6] have concluded that wear could be controlled by altering the microstructure of glass ceramics. Therefore, determination of the wear rate and friction coefficient of A–W glass ceramic is of scientific and technological importance since the understanding of tribological performance may extend the utilization of this material in potential dental applications.

The nature of the crystallinity and distribution of the crystalline phase(s) formed during crystallization depends also on the kind and amount of nucleating agent used. Studies [7,8] have revealed that TiO_2 is a good nucleation agent in many silicate systems. However, the role of TiO_2 as a nucleation agent in A–W glass ceramics has been overlooked due to the fact that the chemical composition includes P_2O_5 and F to promote nucleation. Although there have been some investigations [3,9,10] on the formation, structure, and properties of A–W glass ceramics, data on the crystallization kinetics of these materials are rare. Likitvanichkul and Lacourse [11] reported the effect of glass powder size on the crystallization kinetics of the A–W glass ceramic. Nevertheless, effect of TiO_2 on the crystallization kinetics and tribological properties of this system has not been reported in open literature.

The purpose of the present research is two-fold. The first one is to investigate the role of TiO_2 as nucleating agent in the MgO–CaO–SiO_2–P_2O_5–F system. The second one is to determine the influence of small amount of TiO_2 additions on the crystallization kinetics using non-isothermal differential

* Corresponding author. Tel.: +90 312 210 5932; fax: +90 312 210 2518.
E-mail addresses: parkjongee@daum.net, e127227@metu.edu.tr (J. Park).

0040-6031/$ – see front matter © 2008 Elsevier B.V. All rights reserved.
doi:10.1016/j.tca.2008.01.018

Table 1
Weight percent chemical composition of the glasses investigated

Glass number	MgO	CaO	SiO_2	P_2O_5	CaF_2	TiO_2
1	4.60	44.70	34.00	16.20	0.50	0
2	4.51	43.81	33.32	15.88	0.49	2
3	4.42	42.91	32.64	15.55	0.48	4
4	4.23	41.12	31.28	14.90	0.46	8
5	4.05	39.34	29.92	14.26	0.44	12

thermal analysis (DTA) and on the tribological properties of a glass in this system. Results were supplemented by the phase and microstructural analyses to elucidate the behavior observed.

2. Experimental

The nominal compositions of the glasses investigated are presented in Table 1. A bioactive glass of composition #1 in Table 1, *Glass 1*, was selected as the base composition. This glass has the same composition as the glass developed by Kokubo et al. [1]. In addition to this composition four other compositions of progressively higher TiO_2 content were melted and evaluated.

Glasses were prepared from analytical grade SiO_2, MgO, $CaCO_3$, $CaHPO_4{\cdot}H_2O$, P_2O_5, CaF_2, and TiO_2. Homogeneous mixtures of batches of about 15 g were prepared by mixing the chemicals in a glass jar. No heat treatment was applied prior to melting batches. Premixed powders were melted in a platinum crucible at approximately 1500 °C for 1 h in normal laboratory conditions without controlling the atmosphere. When melting was complete, the melts were poured onto a stainless steel plate of room temperature to form bulk glasses. The as cast glasses were immediately annealed at a temperature of 600 °C for 1 h.

The as cast glasses were crushed using an agate mortar and pestle prior to the differential thermal analysis. The size of the glass powders ranged from 500 to 850 μm. DTA was performed using a differential thermal analyzer (Labsys DTA, Setaram, France) with Al_2O_3 as reference material. DTA scans were obtained at heating rates of 5, 10, 15 and 20 °C/min in a flowing nitrogen atmosphere. The value of the glass transition temperature T_g, crystallization onset temperature T_c, and peak maxima of the crystallization exotherm T_p, were determined from the DTA scans.

The crystallization kinetic parameters were determined using the modified Johnson–Mehl–Avrami equation [12]

$$\ln\left(\frac{\varphi}{T_p^2}\right) = -\left(\frac{E}{R\cdot T_p}\right) + \ln(\upsilon) - \ln\left(\frac{E}{R}\right) \quad (1)$$

where φ is the heating rate, R is the gas constant, E is the activation energy for crystallization, and υ is the frequency factor.

The Avrami parameter, n, which is related to the mechanism of the crystallization process, is determined from the crystallization exotherm using the equation given by Augis and Bennett [13]

$$n = \frac{2.5\cdot R\cdot T_p^2}{\Delta T\cdot E} \quad (2)$$

where ΔT is the width of the crystallization peak at half maximum.

The crushed glasses with the particle size range of 500–800 μm were heat treated in an electric furnace in air at 780 °C for 1 h for nucleation and then at 900 °C for 30 min for crystal growth. The heating and cooling rates were 5 °C/min. Phases formed in the crystallized counterparts of the glasses were identified by X-ray diffraction (XRD) using Rigaku Geigerflex-Dmak/B, Japan with Cu Kα radiation. Scans were run from diffraction angles (2θ) between 20° and 50° at a speed of 2°/min with a 2θ-step of 0.02°.

Bulk glasses were heat treated with same condition as the glass powders. A Jeol 6400 Japan, scanning electron microscope (SEM) was employed to examine the crystal morphology of the crystallized bulk glasses. The samples were mounted in epoxy resin and ground flat by using 240, 400, 800 and 1200 grit abrasive papers consecutively and then polished with diamond paste of 1 μm to achieve a mirror-like surface finish. The samples were etched with 0.05N HCl solution for 1 min before SEM examinations.

The tribological tests were performed on the crystallized bulk glasses with a load of 10 N, rotating speed of 0.25 cm/s, sliding distance of 50 m. Lubrication was not applied to avoid the complication of tribo-chemical effects. The wear track diameter was 1 cm. A pin-on-disk tribometer (CSM Instruments, Switzerland) was employed to conduct tribological tests in accord with ASTM G99-95a standard [14]. A high purity zirconia ball was chosen as the counterface material since it has a higher hardness and lower specific wear rate than the materials studied. After each individual tribological test, the surface profile of the sample was measured by using a stylus profilometer (Surtronic 3+, Taylor Hobson Precision Ltd., England) to determine the wear track depth and wear area. The cross-sectional area of the wear track was calculated by averaging the wear area of four points of maximum mutual distance (90° spacing) on the wear track of the disk following the wear test, from the profiles recorded at the four locations. Wear volume was then calculated by multiplying the cross-sectional area of the wear track by the circumference of the track.

3. Results

The glass compositions investigated were suitable for casting after 1 h of melting at 1500 °C. The as-prepared glass pieces of different compositions were transparent and indicated no crystalline inclusions as determined by X-ray diffraction analysis.

Crystalline phases formed during crystallization of the glass were identified by X-ray powder diffraction (XRD) analysis. XRD pattern of the crystallized counterpart of the as-prepared glasses (glass ceramics) suggested that apatite (JCPDS #9–432) and/or wollastonite (JCPDS #10–489) were precipitated in these glasses depending upon the crystallization heat treatment temperature.

XRD patterns of *Glass 1* after heat treatment at temperatures of 740, 760, 780, 800 and 820 °C for 1 h are shown in Fig. 1. Apatite phase was detected as the only crystalline phase in the patterns taken at temperatures of 760 °C and 780 °C.

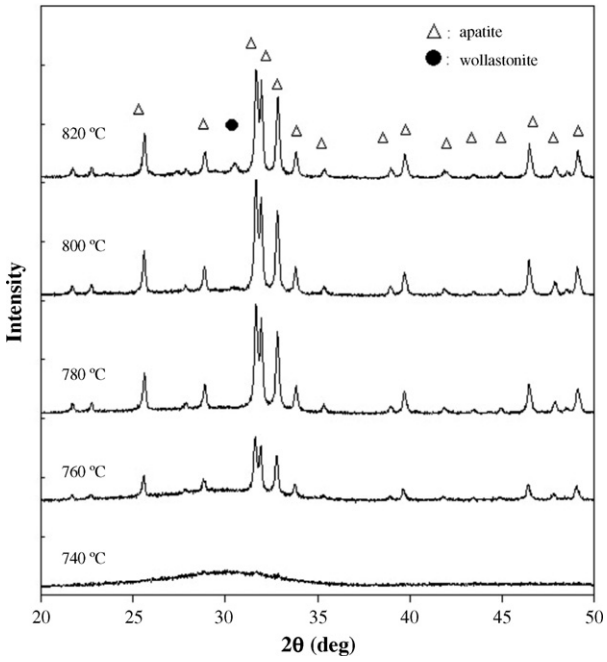

Fig. 1. XRD patterns of *Glass 1* after heat treatment 1 h at different temperatures.

Wollastonite phase started to precipitate at approximately 800 °C.

TiO_2 content in the glass compositions did not have a profound effect on the number of the crystalline phases precipitated. The XRD patterns taken after 1 h heat treatment at 780 °C for *Glass 1* and *Glass 3* indicate the presence of only apatite crystals in both of the glasses as shown in Fig. 2. Fig. 3 illustrates the XRD pattern of *Glass 1* and *Glass 3* after heat treatment at 780 °C for 1 h followed by at 900 °C for 30 min. Precipitation of wollastonite is clearly seen in the patterns.

Representative DTA thermographs taken at a heating rate of 10 °C/min for the glasses containing various amounts of TiO_2 are shown in Fig. 4. The thermographs exhibit two well-defined crystallization exotherms. Influence of the scan rate on the glass transition temperature T_g, and peak maxima of the crystallization exotherm T_p, as well as the thermal stability parameter $T_c - T_g$, is given in Table 2 for all of the glasses investigated.

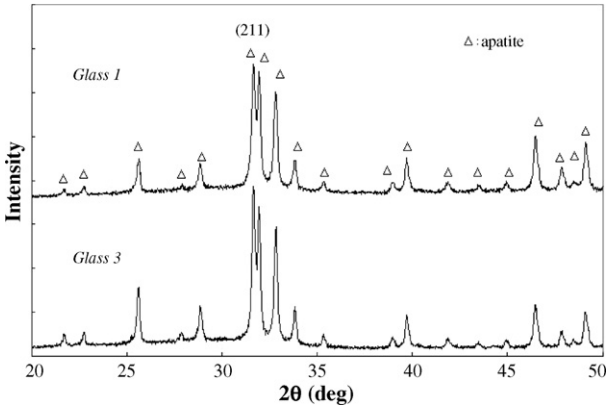

Fig. 2. The XRD patterns of *Glass 1* and *Glass 3* after heat treatment 1 h at 780 °C.

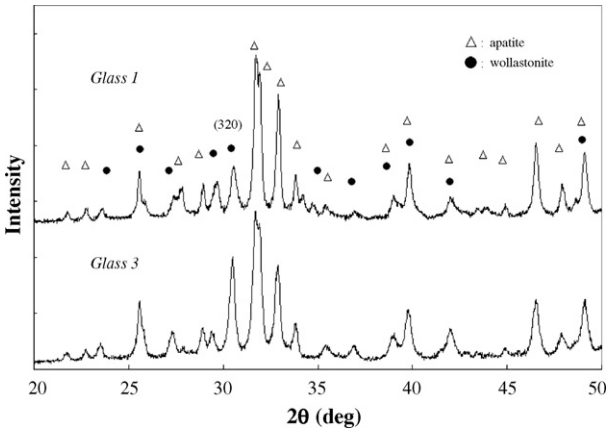

Fig. 3. The XRD patterns of *Glass 1* and *Glass 3* after heat treatment 1 h at 780 °C followed by 30 min 900 °C.

Figs. 5 and 6 show the $\ln(\varphi/T_p^2)$ versus $1/T_p$ plots for apatite and wollastonite, respectively. The solid lines are the least squares fit of the data points. The kinetic parameters E and υ were determined from the slope and intercept, respectively, of a modified form of JMA plots. Values of n were computed from Eq. (2). The values of the kinetic parameters for apatite and wollastonite for all of the glasses investigated are given in Table 3. The maximum uncertainty in measurements was calculated using error analysis as ±15 kJ/mol and ±0.1, for E and n, respectively.

The variation of E for apatite and wollastonite with TiO_2 additions is graphically shown in Fig. 7. Both phases exhibit similar behavior with increasing TiO_2 additions. The E of apatite and wollastonite first decreases and forms minima at about 4 wt% TiO_2 addition and then increases with further TiO_2 additions.

The variation of n for apatite and wollastonite with TiO_2 additions is shown in Fig. 8. The n of apatite and wollastonite tends to increase with TiO_2 additions, forms maxima at about 4 wt% TiO_2 addition and then decreases with further TiO_2 additions.

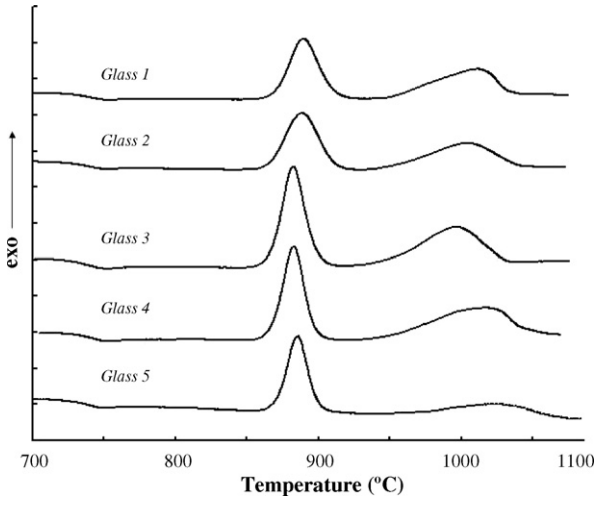

Fig. 4. DTA curves of the glasses investigated. The curves were obtained at the heating rate of 10 °C/min.

Table 2
Values of thermal parameters obtained from DTA for different heating rates for the glasses investigated

Glass number	$\varphi = 5\,^{\circ}$C/min					$\varphi = 10\,^{\circ}$C/min					$\varphi = 15\,^{\circ}$C/min					$\varphi = 20\,^{\circ}$C/min				
	T_g	T_{pA}	T_{pW}	$T_{cA} - T_g$	T_{cW}-T_g	T_g	T_{pA}	T_{pW}	$T_{cA} - T_g$	$T_{cW} - T_g$	T_g	T_{pA}	T_{pW}	$T_{cA} - T_g$	$T_{cW} - T_g$	T_g	T_{pA}	T_{pW}	$T_{cA} - T_g$	T_{cW}-T_g
1	731	884	989	118	195	734	895	1016	127	216	735	909	1022	133	217	737	917	1031	139	226
2	731	881	987	116	186	732	893	1013	127	210	734	906	1018	133	215	736	913	1029	138	217
3	726	875	982	115	186	730	886	1003	125	206	733	897	1016	131	210	735	904	1025	134	214
4	728	876	998	118	189	731	888	1020	126	209	735	898	1029	131	211	737	906	1052	135	224
5	730	876	999	119	189	732	891	1025	130	216	735	900	1039	134	218	738	908	1061	136	232

Subscript A and W designate the crystallization exotherm of apatite and wollastonite, respectively.

Table 3
Activation energy for crystallization (E), Avrami parameter (n), and frequency factor (υ) for apatite and wollastonite

Glass number	$E \pm 15$ (kJ/mol)		$n \pm 0.1$		υ (s^{-1})	
	Apatite	Wollastonite	Apatite	Wollastonite	Apatite	Wollastonite
1	460	443	3.1	1.5	1.74×10^{22}	2.25×10^{17}
2	425	395	3.2	1.5	2.31×10^{21}	4.14×10^{16}
3	408	320	3.3	1.9	9.24×10^{17}	8.32×10^{11}
4	414	351	3.3	1.8	9.59×10^{19}	2.67×10^{12}
5	426	417	3.3	1.5	2.28×10^{21}	6.55×10^{15}

The SEM micrographs in Figs. 9 and 10 illustrate the typical microstructure of the crystallized counterpart of *Glass 1* and *Glass 3*, respectively.

The change of morphology by TiO_2 addition induced the change of tribological properties. Typical SEM micrographs of the wear track obtained from *Glass 1* and *Glass 3* are shown in Fig. 11. Wear debris in the form of glass-ceramic particles or blocks were observed on the wear tracks. The wear rate and friction coefficient of *Glass 1* and *Glass 3* were presented in Table 4.

4. Discussion

The XRD analysis of *Glass 1* revealed that the glass was totally amorphous after heat treatment 1 h at 740 °C as revealed by XRD pattern in Fig. 1. Precipitation of apatite phase started at approximately 760 °C. The XRD pattern taken at 780 °C suggests that apatite is the only crystalline phase. Therefore, the nucleation temperature applied during crystallization heat treatment was taken as 780 °C. The findings are concomitant with the results of Shyu and Wu [9] who have taken nucleation temperature as 755 °C for a glass system similar in chemical composition.

As seen in Fig. 2, the peak intensity of the (2 1 1) plane of apatite crystals at 2θ of ~31.6° in *Glass 3* is noticeably higher than in *Glass 1*, suggesting that the apatite crystals precipitated in *Glass 3* better than in *Glass 1*. The patterns in Fig. 3 suggest that apatite and wollastonite precipitated mutually in these glasses when they are exposed to a temperature of 900 °C. However, crystallization of wollastonite was more dominant in

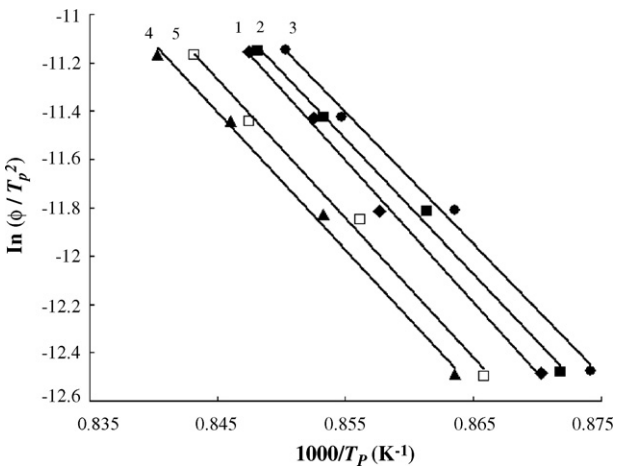

Fig. 5. The $\ln(\varphi/T_p^2)$ vs. $1/T_p$ curves for apatite. Numbers on the curves correspond to the glass numbers given in Table 1.

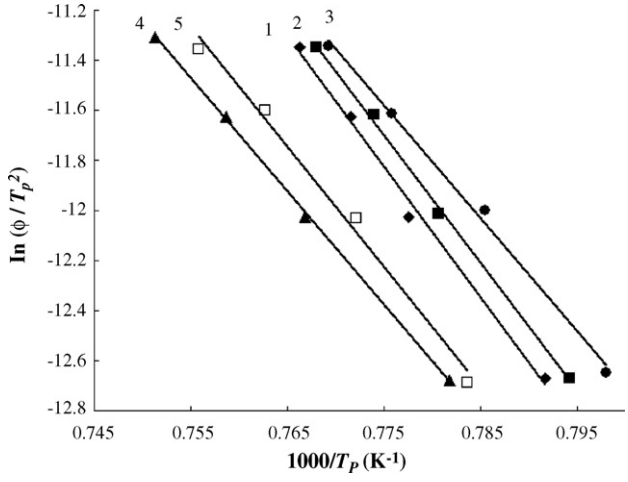

Fig. 6. The $\ln(\varphi/T_p^2)$ vs. $1/T_p$ curve for wollastonite. Numbers on the curves correspond to the glass numbers given in Table 1.

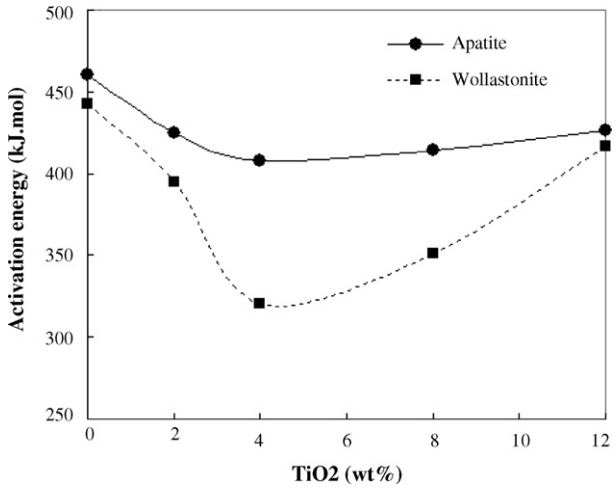

Fig. 7. Variation of the activation energy for crystallization with TiO_2 additions.

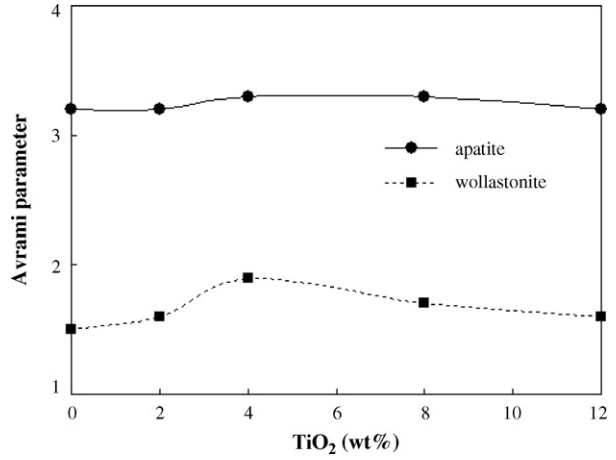

Fig. 8. Variation of Avrami parameter with TiO_2 additions.

Glass 3 as compared to *Glass 1*. The peak intensity of the (3 2 0) plane of wollastonite crystals at 2θ of ~30.5° in *Glass 3* is evidently higher than *Glass 1*. The results reveal that small amount of TiO_2 additions promoted the crystallization of apatite and wollastonite.

The DTA thermographs shown in Fig. 4 imply that at least two crystalline phases are being formed when this glass is reheated.

Table 4
Tribological data of *Glass 1* and *Glass 3*

Glass number	Wear rate (10^{-4} mm^3/Nm)	Wear volume (μm^3)	Friction coefficient (μ)
1	1.8 ± 0.1	3250	0.87
3	0.9 ± 0.2	1520	0.77

The XRD analyses suggested that the first exothermic peak, which occurred in the temperature range of 860–930 °C, is for the crystallization of apatite, and that the second exothermic peak, in the temperature range of 950–1050 °C, is for the crystallization of wollastonite. The findings are in accord with those reported in the literature [3,11]. The crystallization peak for apatite is narrow and sharp but that for wollastonite is broad indicating that the two crystalline phases have different crystallization mechanisms. Ray and Day [15] reported that a sharp peak is characteristic of the bulk crystallization process; whereas, a broad peak reflects the process of surface crystallization.

The incorporation of small amount of TiO_2 to *Glass 1* had an influence on the thermal and stability parameters of the phases crystallized for a given heating rate. As seen in Table 2, the values of the thermal parameters decreased until 4 wt% TiO_2 addition and then increased with further TiO_2 additions. The temperature difference $T_c - T_g$ is used as an indication of the thermal stability of glasses. The higher the value of this difference is, the more the delay in the nucleation process and hence the more the stability of glass is [16–18]. From that point of view, crystallization tendency of the glasses was improved with 4 wt% TiO_2 addition but got worse when TiO_2 concentration was increased further.

Several researchers [18–21] have realized that TiO_2 acts as the glass network former in the form of $[TiO_4]$, whereas others [22–24] have found that TiO_2 acts as the glass modifier in the form of $[TiO_6]$. McMillan [25] reported that TiO_2 would be normally expected to have a co-ordination number of six because of the size of the titanium ion (0.68 Å). However, the titanium ions may have a co-ordination number of four in order to take part in the glass network structure and to be compatible with the silicate network at high temperature [18]. During rapid cooling of the melt, TiO_2 may be "frozen in" with co-ordination number of

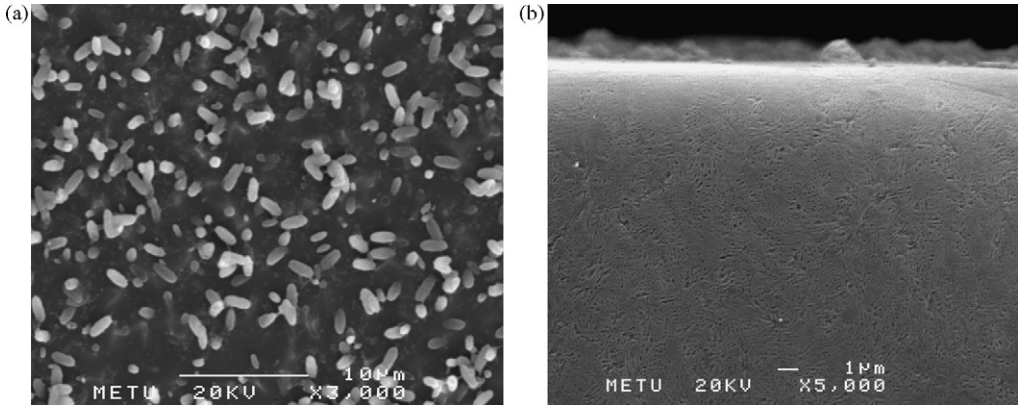

Fig. 9. SEM micrographs of *Glass 1* after heat treatment (a) at 780 °C for 1 h, and (b) at 780 °C for 1 h followed by 900 °C for 30 min.

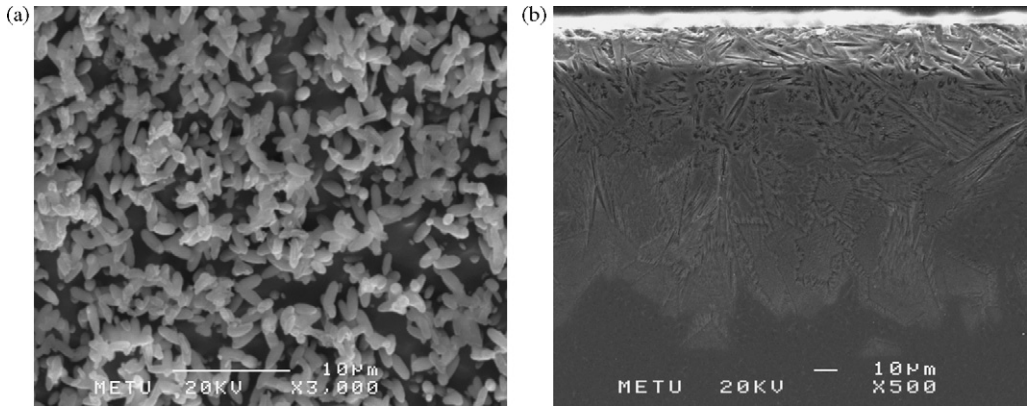

Fig. 10. SEM micrographs of *Glass 3* after heat treatment (a) at 780 °C for 1 h, and (b) at 780 °C for 1 h followed by 900 °C for 30 min.

four, so if there is a reheating on the glass, the tendency will be for TiO_2 to assume the co-ordination number of six and in doing this it will no longer be able to occupy network-forming positions [25]. The tetrahedral [TiO_4] enhances the glass formation ability by networking with [SiO_4] groups, and does not induce the formation of any non-bridging oxygen ions. However, octahedral [TiO_6] exists in six-fold co-ordination and loosens the glass network. This may be one of the reasons for the initial decrease and subsequent increase in the thermal parameters with increasing TiO_2 additions. From the results obtained, it is obvious that TiO_2 functioned as the glass network modifier and broke up the random network of glass producing the non-bridging oxygen when it is added to the base glass up to 4 wt%. Nevertheless, it functioned as the glass network former enhancing the glass formation when further additions were made. The initial decrease until 4 wt% TiO_2 addition followed by an increase in the E of apatite and wollastonite supports the explanation for the possible effect of TiO_2. As seen in Table 3, the E for apatite and wollastonite is 460 ± 15 and 443 ± 15 kJ/mol, respectively, in *Glass 1*, and becomes 408 ± 15 and 320 ± 15 kJ/mol, respectively, in *Glass 3*. The decrease in E with 4 wt% TiO_2 addition is interpreted as the indication of the increasing tendency for crystallization [26]. Although it is difficult to find the physical meaning of the activation energy precisely when bulk and surface crystallization occur simultaneously [27], lower value of E in *Glass 3* as compared to *Glass 1* imply that *Glass 3* is less stable and have higher tendency to devitrification. It is evident that TiO_2 promotes the crystallization of not only apatite but also wollastonite. Thus, it is an effective nucleation agent for the glasses in the $MgO–CaO–SiO_2–P_2O_5–F$ system.

The n is a crystal growth index, which can describe the crystallization reaction mechanism and ability of a glassy material to crystallize. The crystallization process becomes easier when the value for n is higher [26]. When n is less than 3, surface crystallization is the dominant crystallization mechanism whereas; n greater than 3 means bulk crystallization mechanism is dominant [15]. The values for n for apatite and wollastonite in *Glass 1* are 3.2 ± 0.1 and 1.5 ± 0.1, respectively. It is obvious that apatite prefers to crystallize through bulk crystallization three-dimensional growth mechanism and wollastonite crystallizes through surface crystallization two-dimensional growth mechanism. The values for n for apatite and wollastonite increase slightly from 3.1 ± 0.1 to 3.3 ± 0.1, and from 1.5 ± 0.1 to 1.9 ± 0.1, respectively, when 4 wt% TiO_2 is incorporated. As shown in Fig. 8, the n for apatite and wollastonite show similar trend with increasing TiO_2 additions. In effect, TiO_2 additions tended to enhance the three-dimensional bulk crystallization mechanisms of apatite phase. The incorporation of small amount of TiO_2 (up to 4 wt%) encouraged the crystallization mechanisms of wollastonite from one-dimensional surface crystallization to two-dimensional surface crystallization while

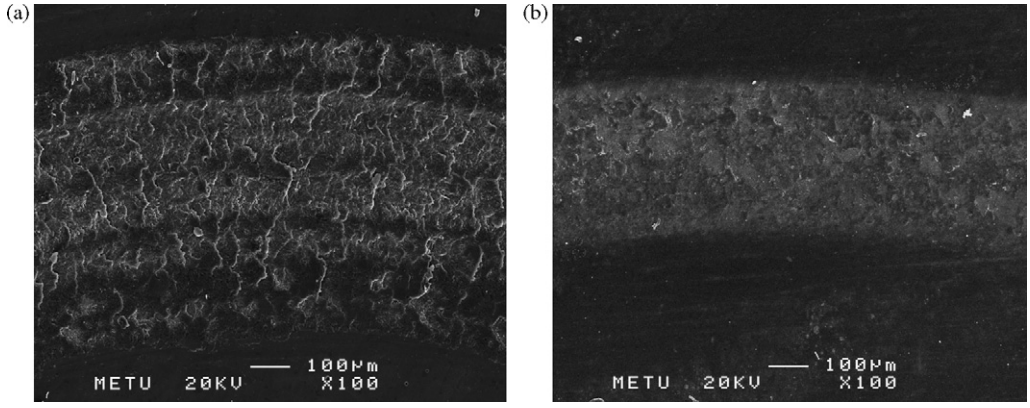

Fig. 11. SEM micrographs of the wear track for (a) *Glass 1* and (b) *Glass 3*.

further additions had a tendency towards one-dimensional surface crystallization [11,26].

The SEM micrographs in Fig. 9 reveal that apatite crystals are uniformly precipitated by consuming the glass matrix surrounding them. The nominal length of the rice-shaped crystals is approximately 2 μm. As the heat treatment temperature increased, the crystals grew and appeared in web-like microstructure. Dentric growth of the apatite crystals in the glass ceramic has been also observed by Kokubo [3]. The apatite crystals are well precipitated in *Glass 3* as shown in Fig. 10. The length of the crystals is more or less the same with *Glass 1*, but the number of apatite crystals per unit volume increases. The results are compatible with the results of the XRD study. The rich precipitation of apatite in this glass is attributed to decrease in E of apatite with increasing TiO_2 addition. In addition to apatite crystals, the wollastonite crystals are formed as needle shape after heat treating the glass at 780 °C for 1 h followed by at 900 °C for 30 min. Wollastonite crystallizes through surface crystallization mechanism. Hence, the crystals grow from the surface towards the interior as shown in Fig. 10(b). The needle-like wollastonite crystals have not been observed in *Glass 1* because they are crystallized between apatite grains. However, extensive crystallization of wollastonite has been observed in *Glass 3* because it has low E for wollastonite. It is obvious that addition of as small as 4 wt% TiO_2 to *Glass 1* encouraged apatite and wollastonite crystallization.

As shown in Fig. 11, *Glass 3* has relatively thin wear track than *Glass 1* for the identical experimental conditions. Wear debris in the form of glass-ceramic particles or blocks were observed on the wear tracks, implying that abrasive and adhesive wear mechanisms have occurred during wear test.

The wear rate and friction coefficient of *Glass 1* decreased from 1.8 ± 0.1 to 0.9 ± 0.2 and 0.87 to 0.77, respectively, with 4 wt% TiO_2 addition. The decrease in the wear rate and friction coefficient is attributed to the existence of more wollastonite crystals which prohibit the wear of materials. It has been shown that the whisker-like wollastonite crystals in A–W glass ceramic enhance the mechanical properties [3] by bringing reinforcement effect in matrix [28]. It is obvious that, presence of more wollastonite phase generates unique resistance to wear in A–W glass ceramics. Another reason for the improvement in the tribological properties may be the formation of compressive stress induced from the surface crystallization process.

5. Conclusions

(1) Bulk and surface crystallization occurred in the glasses composed of the system MgO–CaO–SiO_2–P_2O_5–F. The crystallization mechanism of apatite is a three-dimensional bulk process whereas that of the wollastonite is a two-dimensional surface process. Small amount of TiO_2 additions did not have much influence on, but aided the crystallization mechanisms of apatite and wollastonite.
(2) With respect to apatite and wollastonite, as the TiO_2 content increases (up to 4 wt%), the activation energies decrease to a minimum of 408 and 320 kJ/mol, respectively, implying that TiO_2 is an effective nucleating agent for promoting the crystallization of apatite and wollastonite.
(3) It is possible to alter the wollastonite content and hence the tribological properties of the apatite–wollastonite glass ceramics by changing the TiO_2 content.

Acknowledgements

This work was funded and supported partially by Middle East Technical University, METU, Research Fund Projects, Project Number: BAP-2005-07-02-00-90.

References

[1] T. Kokubo, M. Shigematsu, Y. Nagashima, M. Tashiro, T. Nakamura, S. Higashi, Bull. Inst. Chem. Res. Kyoto Univ. 60 (1982) 260–268.
[2] T. Kokubo, S. Ito, M. Shigematsu, J. Mater. Sci. 20 (1985) 2001–2004.
[3] T. Kokubo, Biomaterials 12 (1991) 155–163.
[4] W. Höland, V. Rheinberger, E. Apel, C. Hoen, M. Höland, A. Dommann, M. Obrecht, C. Mauth, U. Graf-Hausner, J. Mater. Sci.: Mater. Med. 17 (2006) 1037–1042.
[5] M. Kalin, S. Jahanmir, Wear 255 (2003) 669–676.
[6] S. Jahanmir, X. Dong, Wear 181–183 (1995) 821–825.
[7] M. Rezvani, B. Eftekhari-Yekta, M. Solati-Hashjin, K. Marghussian, Ceram. Int. 31 (2005) 75–80.
[8] C.H. Gur, A. Ozturk, J. Non-Cryst. Solids 351 (2005) 3655–3662.
[9] J.J. Shyu, J.M. Wu, J. Am. Ceram. Soc. 73 (1990) 1062–1068.
[10] J. Park, A. Ozturk, Mater. Lett. 61 (2006) 1916–1921.
[11] S. Likitvanichkul, W.C. Lacourse, J. Mater. Sci. 33 (1998) 5901–5904.
[12] H.E. Kissinger, Anal. Chem. 29 (1957) 1702–1706.
[13] J.A. Augis, J.E. Bennett, J. Therm. Anal. 13 (1978) 283–292.
[14] ASTM G99-95a, Standard test method for wear testing with a pin-on-disk apparatus, ASTM International, 2002, 414–419.
[15] C. Ray, D.E. Day, J. Am. Ceram. Soc. 73 (1990) 439–442.
[16] S. Mahadevan, A. Giridhar, A.K. Singh, J. Non-Cryst. Solids 88 (1986) 11–34.
[17] N. Mehta, R.S. Tiwari, A. Kumar, Mater. Res. Bull. 41 (2006) 1664–1672.
[18] A. Goel, E.R. Shaban, F.C.L. Melo, M.J. Ribeiro, J.M.F. Ferreira, J. Non-Cryst. Solids 353 (2007) 2383–2391.
[19] H.F. Wu, C.C. Lin, P.Y. Shen, J. Non-Cryst. Solids 209 (1997) 76–86.
[20] R.B. Rao, D.K. Rao, N. Veeraiah, Mater. Chem. Phys. 87 (2004) 357–369.
[21] P.N. Rao, C.L. Kanth, D.K. Rao, N. Veeraiah, J. Quant. Spectrosc. Ra. 95 (2005) 373–386.
[22] A. Shaim, M. Et-tabirou, Mater. Chem. Phys. 80 (2003) 63–67.
[23] L. Koudelka, P. Mosner, M. Zeyer, C. Jager, J. Non-Cryst. Solids 326–327 (2003) 72–76.
[24] S.H. Byeon, S.O. Lee, H. Kim, J. Solid State Chem. 130 (1997) 110–116.
[25] P.W. McMillan, Glass Ceramics, Academic Press, London, 1964, pp. 63–64.
[26] B. Yu, K. Liang, A. Hu, S. Gu, Mater. Lett. 56 (2002) 539–542.
[27] K. Matusita, S. Sakka, Bull. Inst. Chem. Res. 59 (1981) 159–171.
[28] J. Tong, Y. Ma, M. Jiang, Wear 255 (2003) 734–741.